Global Change Biology (2006) **12,** 1–11, doi: 10.1111/j.1365-2486.2006.01268.x

Global spatial patterns and temporal trends of burned area between 1981 and 2000 using NOAA-NASA Pathfinder

D. RIAÑO*†, J. A. MORENO RUIZ*‡, D. ISIDORO§ and S. L. USTIN*

**Center for Spatial Technologies and Remote Sensing (CSTARS), University of California, 250-N, The Barn, One Shields Avenue, Davis, CA 95616-8617, USA, †Departamento de Geografía, Universidad de Alcalá, Colegios 2, E-28801 Alcalá de Henares, Madrid, Spain, ‡Departamento de Lenguajes y Computación, Universidad de Almería, 04120 Almería, Spain, §Unidad de suelos y riegos, Centro de Investigación y Tecnología Agroalimentaria de Aragón (CITA-DGA), PO Box 727, 50080 Zaragoza, Spain*

Abstract

An analysis of the spatial and temporal patterns of global burned area with the Daily Tile US National Oceanic and Atmospheric Administration-Advanced Very High-Resolution Radiometer Pathfinder 8 km Land dataset between 1981 and 2000 is presented. Nine distinct temporal and spatial fire patterns were identified at the global scale using principal components and cluster analysis. Three major fire seasons were identified from June to December and from February to June for different areas of the northern hemisphere and from October to March for the southern hemisphere. The area burned primarily followed the annual cycle and secondarily, an important 6-month cycle. Temporal cycles were unimportant in some equatorial and tropical areas in the northern hemisphere. The total annual burned area has not increased in the last 20 years but a significant increase was found in the mid-latitude and subtropical areas of the northern hemisphere which was offset by a slight decrease in burned area in tropical southeast Asia and Central America. Additionally, burned area has significantly increased during the summer in the mid-latitudes of the northern hemisphere and in the boreal region, and the fire season starts earlier in the mid-latitudes. Total burned area was explained by the extent of savanna (wooded grassland) cover. Latitude was not determinative as divergent fire patterns were encountered and did not have an impact on extent of burned area at our spatial level of analysis.

Nomenclature:

ARIMA	=	autoregressive integrated moving average
AVHRR	=	Advanced Very High-Resolution Radiometer
CL	=	cluster group
GAC	=	NOAA-AVHRR global area coverage
MODIS	=	moderate resolution imaging spectrometer
n	=	number of cases for each specific analysis
NOAA	=	US National Oceanic and Atmospheric Administration
P	=	probability of a significant trend
PAL	=	NOAA-AVHRR Pathfinder Land 8-km land dataset
PC	=	principal component
Q	=	Mann–Kendall seasonal nonparametric estimator of slope
SD	=	standard deviation
SE	=	standard error

Keywords: burned area, fire frequency, global, NOAA-AVHRR pathfinder land, principal components, temporal trends

Received 6 January 2005; revised version received 23 December 2005 and accepted 26 June 2006

Correspondence: Present address: David Riaño, Center for Spatial Technologies and Remote Sensing (CSTARS), University of California, 250-N, The Barn, One Shields Avenue, Davis, CA 95616-8617, USA, tel. +1 530 752 5092, fax +1 530 754 5491, e-mail: driano@cstars.ucdavis.edu

Introduction

Calculating the area burned is the most critical parameter used to calculate biomass consumed in wildfires. However, total burned biomass depends not only on the burned area, but also on pre-existing biomass and burning efficiency (Seiler & Crutzen, 1980). Better knowledge of spatial patterns and temporal trends in global burned area together with information about biomass consumption, can lead to more accurate estimation and prediction of global atmospheric emissions from wildfires. About 32% of the carbon monoxide and 40% of the carbon dioxide released to the atmosphere globally come from burned biomass (Levine, 1996). This atmospheric forcing is a driver for climate warming and can have positive feedback with increased fire frequency (IPCC, 2000).

Analysis of burned area and biomass consumed at the intercontinental scale was traditionally made using statistics from the Food and Agriculture Organization (Hao & Liu, 1994). Since the late 1970s, analyses have only partially utilized remote sensing data, mainly for regional estimates, using single date Landsat Multi-Spectral Scanner (Lanly, 1982), which has a 79 m spatial resolution in 185 km × 185 km images. The Lanly study used diverse sources of data, including remote sensing information only for some regions, short time series records, along with different data processing techniques which provided inconsistent and incomplete burned area datasets.

A single remote sensing data source can provide globally coherent multitemporal spatial information, not only from the visible part of the spectrum but also reflected solar infrared, which can be used to obtain consistent environmental monitoring at the global scale (Townshend *et al*., 1991). Since 1979 the US National Oceanic and Atmospheric Administration (NOAA) has launched a series of polar orbiting satellites carrying the Advanced Very High-Resolution Radiometer (AVHRR). The images from five spectral bands in the red, near-infrared, middle-infrared and thermal-infrared are acquired twice daily, and have a spatial resolution of 1.1 km at nadir. This instrument meets the criteria for generating maps of burned area at the global scale, by providing recurring and systematic low spatial, high temporal resolution data that has now accumulated a long time series. Several authors have generated statistics about the global distribution of active fires based on 1-year data (Dwyer *et al*., 1998, 2000 a,b; Stroppiana *et al*., 2000). Active fires provide accurate information on the timing of the fire, important for short-term atmospheric emission modelling, but which usually underestimate the extent of the burned area (Simon *et al*., 2004).

Moreno Ruiz *et al*. (1999) used the original NOAA-AVHRR Pathfinder Land (PAL) 8-km land dataset to produce a global information system for burned area detection for the year 1990. NASA discovered that this dataset had coding errors in the preprocessing software for computing the solar zenith angle (http://disc.gsfc.nasa.gov/landbio/PAL_coding_errors.pdf). More recently, Carmona-Moreno *et al*. (2005) used the original PAL dataset to analyze the global fire season and its relationship to El Niño events using a 17-year dataset. As could be expected, they found that there were inconsistencies in the original Daily Global PAL dataset due to different zenithal angles measured by the different instruments in the NOAA-AVHRR series. In 2000, NASA Goddard Biosphere program released a new version in which inconsistencies due to zenithal angle were normalized (ftp://disc1.gsfc.nasa.gov/data/avhrr/tile_8km/pal_tile_readme.txt). They also reconfigured the dataset so that the information could be delivered in tiles that represent a 1000 km × 1000 km region.

Two recent initiatives have produced accurate global burned area maps at a finer spatial 1 km resolution than NOAA-AVHRR PAL data but only for the year 2000. One initiative used the Along Track Scanning Radiometer-2 obtaining data with red, near-infrared, shortwave-infrared and thermal-infrared channels on the environmental satellite, as part of the GLOBSCAR project (Simon *et al*., 2004). This project applied two combined algorithms, one contextual, based on spatial differences and the other based on spectral analysis, but without multitemporal thresholds. The other initiative used three System Pour l'Observation de la Terre Vegetation bands in the red, near-infrared, and shortwave-infrared depending on regions of the world, within the GBA2000 project (Gregoire *et al*., 2003). They applied regional algorithms, which complicate the repeatability of the product, mainly using a multitemporal analysis to detect burned area but not spatial differences (Tansey *et al*., 2004). Although both results, GLOBSCAR and GBA2000 were validated with single date Landsat Thematic Mapper data having a 30 m spatial resolution in the optical spectral domain, the intercomparison shows substantial differences (Simon *et al*., 2004).

Spatial and seasonal distribution of active fires at the global scale were determined for a 1.5-year period, between April 1992 and December 1993 (Dwyer *et al*., 2000b). They reported five major seasonal fire patterns in this dataset based on cluster (CL) analysis using spatial and temporal descriptors of the fire season (Dwyer *et al*., 2000a). Their results are important as a prototype but several authors have addressed the need for a high-quality global multiyear dataset of fire events to measure global atmospheric emissions (Kasischke & Penner, 2004; Simon *et al*., 2004) and NOAA-AVHRR

PAL could fill this gap until global time series are available from other sensors with better spectral and spatial resolution.

The trend in current fire research is to operationally produce systematic fire products at the global scale, in order to estimate global atmospheric emissions. An active fire product is being systematically generated globally from the Moderate Resolution Imaging Spectrometer (MODIS) (Justice *et al*., 2002) and a burned area algorithm was developed for this sensor (Roy *et al*., 2005). MODIS has better spatial (250 m–1 km) and spectral (36 bands) resolution than NOAA-AVHRR but the record extends back for only 5 years.

The main purpose of this study was to identify global patterns of burned area using the 20 years of NOAA-AVHRR data which will provide a more consistent spatial and temporal basis for interpretation than statistics compiled from different sources or short periods (e.g. annual studies). This multiyear analysis was done using the reconfigured Daily Tile PAL dataset which has been normalized to account for differences in solar zenithal angles that have occurred due to satellite drift (http://disc.sci.gsfc.nasa.gov/interdisc/readmes/pal_ftp.shtml). We identified the main spatial patterns in global fires by performing a CL analysis on the principal components (PCs) of the time series. Seasonal and interannual burned area patterns were analyzed to obtain fire frequency and periodicity in the burn cycle. We also determined whether burned area increased or decreased for any month or annually over the 20 years at the global scale and for any of the regions identified in the CL analysis. The fire patterns were correlated with environmental variables to explain fire occurrence and frequency such as land cover, spatial distribution, elevation and sea influence.

Materials and methods

The generation of burned area at the global scale was automated from July 1981 to December 2000 on a Daily Tile PAL 8 km dataset. We applied the algorithm proposed by Moreno Ruiz *et al*. (1999) and used to estimate burned area in tropical Africa in 1990, but using the reconfigured Daily Tile PAL data which addressed the solar zenith angle errors. Their method analyzed Normalized Difference Vegetation Index (Rouse *et al*., 1974) that uses the red and the near-infrared bands, derived from the multitemporal algorithm of Barbosa *et al*. (1999). The algorithm also included contextual information and was automated to obtain a probability distribution of burned area.

No data was available from September to December 1994 because the NOAA-11 mission ended September 14, 1994 and NOAA-14 was not launched until January 3, 1995. We also found inconsistencies in January and February 2000 data with abnormally low reflectances for the global data which were also removed from the analysis.

Moreno Ruiz *et al*. (1999) evaluated the burned area method we employed by comparing it to the map of Africa that Barbosa *et al*. (1999) produced from the NOAA-AVHRR global area coverage (GAC) 5 km dataset for the year 1990. Their analysis showed similarity in the seasonality and location of the burned areas although the number of burned pixels identified with the GAC dataset was higher. This difference could be attributed to the change in resolution from 5 to 8 km.

Total number of burned pixels (8 km × 8 km) were grouped into tiles of 125 × 125 pixels (1000 km × 1000 km) and aggregated monthly. Data were standardized two ways to work with fire frequency. First, we calculated the percentage of burned area after compensating for the presence of water pixels in each tile

$$\text{Burned area}\,(\%) = \frac{\text{Fires}}{T_{\text{pixels}} - T_{\text{water}}} \times 100,$$

where Fires is the total number of pixels burned for that tile in that month. T_{pixels} the total number of pixels in the tile = 15 625. T_{water} the total number of pixels of water extracted from the global 1984 NOAA-AVHRR PAL 8 km land cover map (De Fries *et al*., 1998).

Second, the monthly data of all tiles in the series were standardized to compensate for the difference in absolute values between tiles.

PC analysis was run over the monthly series for each tile to reduce the number of variables ($n = 228$) to uncorrelated variables. Tiles were grouped according to the PCs following a CL rule, based on Euclidian distance and Ward's linkage, using Matlab 6.0 (The Math Works, http://www.mathworks.com, USA). Tiles calculated to have a total burned area of less than 10% or had more than 90% water pixels were removed from the study. We retained nine CLs after the PC analysis, considering the linkage distance between CLs and the spatial distribution of the resulting CLs.

Mean and standard error (SE) for the percentage of monthly burned area of all normalized tiles was calculated for each CL. SE was used instead of standard deviation (SD) to compensate for the different number of tiles per CL (n):

$$\text{SE} = \frac{\text{SD}}{\sqrt{n}}.$$

We also calculated the mean and SE for each month, January–December and fire frequency for each CL. A periodogram was built to analyze the fire cycles considering the standardized monthly mean of all tiles

in the CL using Statgraphics Plus 5.0 (Manugistics, http://www.statgraphics.com, USA). Autoregressive integrated moving average (ARIMA) models (Box *et al.*, 1994) were fitted to the mean normalized series for each CL and the best ARIMA models were used to fill gaps in the series (September–December 1994 and January–February 2000). ARIMA models can forecast future behavior based on previous observations of time series data and can incorporate other environmental variables to explain the occurrence of the output variable of interest (Peiris & McNicol, 1996). ARIMA models have been used to predict temporal changes using microwave remote sensing data (Piwowar & Ledrew, 2002). The best ARIMA models were seasonal autoregressive models of orders one or two in the seasonal and non-seasonal components for every CL.

Trends in the number of burned pixels in the period 1981–2000 were estimated globally and for each CL with the Mann–Kendall seasonal test (Gilbert, 1987). This test establishes upward and downward trends in the number of burned pixels each month from the differences between the numbers of burned pixels in the same months of different years. It also detects annual trends from the difference between the numbers of burned pixels in each year and other years. The slopes of trends that were significantly different from 0 at the $\alpha = 0.10$ significance level in a two-tailed test (probability of a significant trend $P > 0.95$) and their 90% confidence intervals were established for each month and for the whole year using the Kendall seasonal slope estimator (Gilbert, 1987).

We evaluated land cover, longitude, latitude, elevation and sea influence to describe fire patterns for each CL. Vegetation, topography, and weather drive fire behavior (Ryan, 2002) and variables that characterize these parameters are included in fire risk models to explain fire occurrence (Chuvieco *et al.*, 1999). Land cover provides a measure of vegetation structure that is ultimately related to conditions for fire spread (Anderson, 1982). The percentage of each land cover type in each CL was calculated following the global 1984 NOAA-AVHRR PAL 8 km land cover map (De Fries *et al.*, 1998). Tiles in each CL were grouped by latitude and longitude to determine whether CLs were responding to the spatial distribution patterns of land cover. Mean and SE longitude and latitude was calculated for each CL using the center location of each tile. Air temperature decreases with elevation (Trewartha *et al.*, 1961) which results in higher fire frequency at lower elevations (Diaz-Delgado *et al.*, 2004). Mean and SE elevation of each tile in each CL were extracted from the global elevation dataset (NGDC, 1993). Coastal areas have lower amplitude of thermal oscillations (Trewartha *et al.*, 1961) and tend to have higher rainfall and relative humidity, all of which reduce fire risk (Verdon *et al.*, 2004). For this reason, sea influence was obtained as percentage of land tiles. A tile was considered land if 90% or more of pixels were not water, based on the global 1984 NOAA-AVHRR PAL 8 km land cover map (De Fries *et al.*, 1998).

Results

The first 15 PCs accounted for 75.06% of the total variance. The subsequent PCs added little additional information, and required an exponential increase in the number of PCs to explain significantly more variance. Because of the potential for overfitting, we chose to keep the number of PCs at 15. The first four PCs represented 53.92% of the total variance and exhibited an annual (PC 1 and PC 2) or a 6-month (PC 3 and PC 4) cycle (Fig. 1), whereas the remaining PCs did not clearly show an annual periodicity (not shown in the figure). PC 1 had a positive weight in December–January and a negative weight in July–August. PC 2 was similar to PC 1 but out of phase, having a positive peak in November and a negative peak in April. PC 3 had two positive weight peaks in April and October and two negative

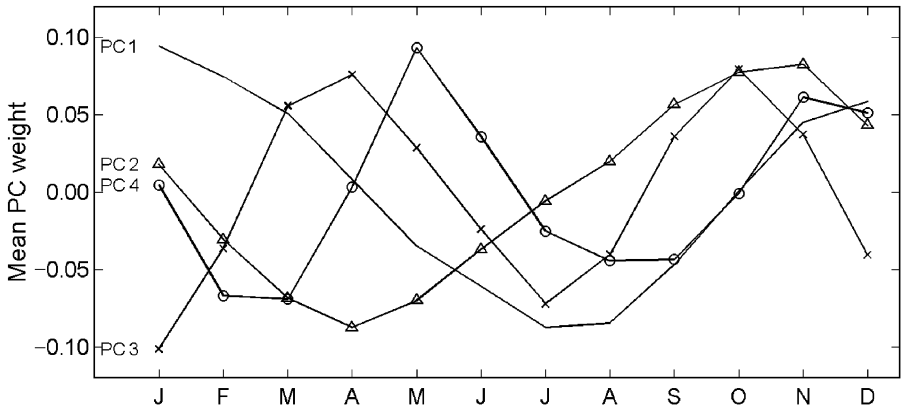

Fig. 1 Mean principal component (PC) eigenvector weights for each month.

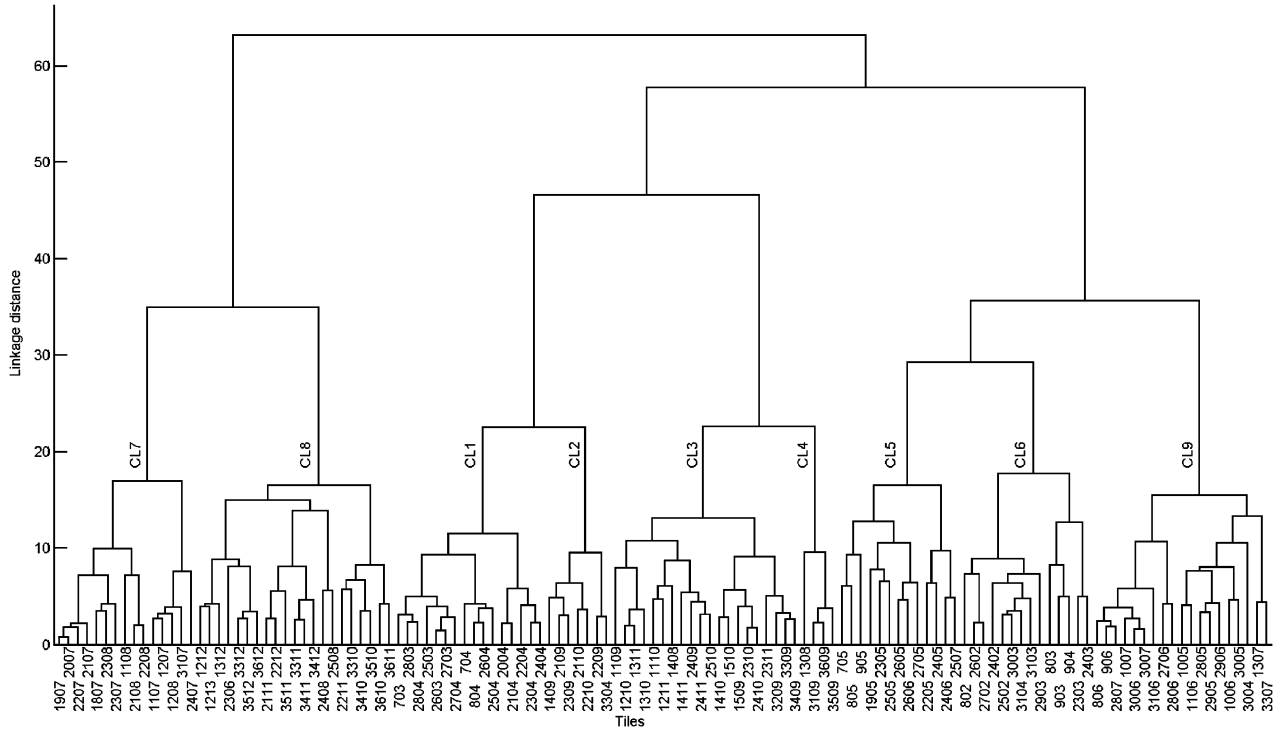

Fig. 2 Cluster (CL) tree built to group tiles from the 20-year advanced very high-resolution radiometer record.

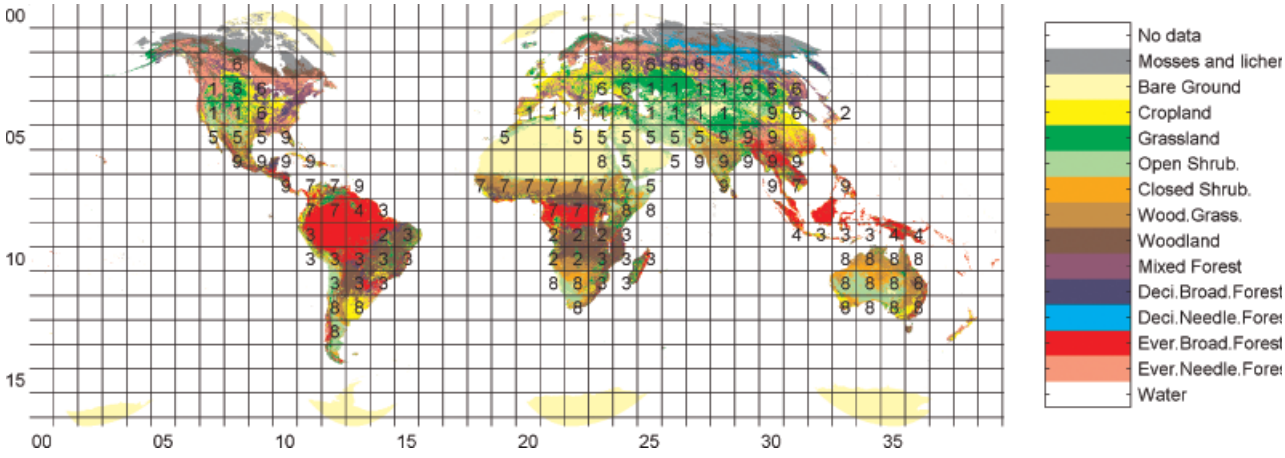

Fig. 3 Global land cover map showing the cluster number for each land cover tile. Map is presented in the interrupted Goode projection divided into 40×18 tiles of 125×125 pixels each.

peaks in January and July. PC 4 was out of phase with PC 3 with two positive weight peaks in May and November and two negative peaks in February–March and August–September.

The CL tree (Fig. 2) illustrates that there are three major global burned area patterns in the 20-year time series: CL 7 and 8; CL 1–4; and CL 5, 6 and 9. CL 1 and 6 explained the fire frequency in the mid-latitudes of the northern hemisphere (Fig. 3); CL 3, 4 and 7 explained the equatorial patterns; CL 2 central-southern Africa; CL 8 the southern hemisphere; and CL 5 and 9 the tropical northern hemisphere.

The timing of the fire regime and cycles for each CL are presented in Fig. 4. The Box–Pierce test demonstrated that the time series for all CL were not random (P-value <0.001), but expressed predominantly annual cycles.

The global trend statistics in the total number of pixels burned in any month or annually were not significantly different from 0, at $\alpha = 0.10$ significance level ($P < 0.95$). Therefore, no significant upward or

Table 1 Probability of a significant trend (P), Mann–Kendall seasonal nonparametric estimator of slope (Q in pixel yr^{-1}) and 90% confidence interval of Q (in brackets) for those months and years that presented a significant trend at the $\alpha = 0.10$ significance level in any cluster ($P > 0.95$)

Month	Cluster 1	Cluster 5	Cluster 6	Cluster 9
January				
P	0.98		0.96	
Q	0.0 pixel yr^{-1} (0.0, 0.1)		0.0 pixel yr^{-1} (−0.0, 0.0)	
March				
P			0.96	
Q			0.3 pixel yr^{-1} (0.0, 1.0)	
June				
P	0.98			
Q	61.9 pixel yr^{-1} (11.6, 130.4)			
July				
P	0.99		0.97	
Q	168.8 pixel yr^{-1} (73.3, 259.2)		52.0 pixel yr^{-1} (9.8, 77.4)	
September				
P		0.97		
Q		26.6 pixel yr^{-1} (3.3, 51.9)		
October				
P			0.98	
Q			1.3 pixel yr^{-1} (0.1, 2.9)	
Year				
P	1.00	0.97		0.98
Q	24.2 pixel yr^{-1} (0.0, 50.3)	9.2 pixel yr^{-1} (0.9, 17.3)		−5.5 pixel yr^{-1} (−11.7, −1.0)

downward global trend was found in the burned area data. In marked contrast, significant trends were found for some individual CL (Table 1).

Table 2 shows the CL for the main land cover types, latitude, longitude, elevation, and sea influence. These variables were also correlated with mean monthly burned area percentage showing that, at this CL level of analysis, land cover is related to mean monthly percent of burned area. More specifically, as the percentage of the savanna (wooded grassland) land cover type increases it is correlated with a higher mean monthly burned area ($R^2 = 0.85$). On the other hand, spatial distribution, elevation and sea influence do not cause differences in burned area at this level of spatial and temporal aggregation.

CL 1 burned mainly in July–August (Fig. 4a) and showed an upward trend in burned area in January, June and July (statistic Z different from 0 with $P > 0.90$; Table 1). The increase in January was small because the number of burned pixels in that month was zero in most years and it is the occurrence of a few burned pixels in the last years of the series that cause this trend. The increase is quite high in June (slope = 62 pixel yr^{-1}) and July (slope = 169 pixel yr^{-1}). The number of burned pixels increased significantly over the whole year (24 pixel yr^{-1}). The dominant CL 1 vegetation type was grassland and tiles were located in Eurasia and western North America (Fig. 3 and Table 2).

CL 2 had a fire season similar to CL 1, but with a larger burned area and an interannual cycle. Upward or downward trends were not significant for any month nor annually. Tiles were located mainly over woodlands in Equatorial and South Africa. A single tile located in Japan caused a large dispersion in latitude values in CL 2 (Table 2).

CL 3 burns mainly occurred later in the year with a peak in September–October and an interannual cycle. Upward or downward trends were not significant for any month or annually. This CL is composed of woodland as the main land cover type. Tiles were located in tropical South America, southeast Africa, Madagascar and Indonesia.

CL 4 maintained a remarkably consistent fire regime of interannual cycles, but with unclear annual periodicity (Fig. 4b), and no upward or downward temporal trends. This type was mainly evergreen broadleaf forest and grouped only in four tiles located in New Guinea, Indonesia and northern South America.

CL 5 also showed a more important interannual than annual cycle. It showed an upward burned area trend in September (statistic Z different from 0 with $P > 0.90$; slope = 27 pixel yr^{-1}). The number of annual burned

Table 2 Variables to explain cluster groups

	Cluster										
Land cover (%)	1	2	3	4	5	6	7	8	9	R^2	*P*-value
Evergreen needleleaf forest	9	1	1	0	2	18	0	0	9	0.23	0.19
Evergreen broadleaf forest	0	17	24	83	0	0	28	2	18	0.02	0.69
Deciduous needleleaf forest	0	0	0	0	0	1	0	0	0	0.16	0.29
Deciduous broadleaf forest	1	8	5	1	0	9	3	0	7	0.01	0.82
Mixed forest	1	0	1	0	1	14	0	0	1	0.15	0.30
Woodland	2	47	39	9	3	4	16	7	12	0.20	0.22
Savanna	3	13	6	0	6	1	23	19	14	0.85	0.00
Closed shrubland	1	2	2	0	5	0	5	21	3	0.20	0.23
Open shrubland	17	1	4	0	33	3	7	26	5	0.00	0.97
Grassland	39	5	8	3	3	23	5	5	14	0.17	0.27
Cropland	11	5	8	3	4	26	8	11	16	0.03	0.63
Bare ground	14	1	1	0	42	1	6	8	0	0.03	0.64
Mosses and lichens	2	0	0	0	0	1	0	0	0	0.26	0.16
Longitude mean*	22	22	19	29	20	22	19	28	22	0.07	0.51
Longitude SE*	1.9	2.1	1.7	5.4	2.0	2.4	1.5	1.8	2.2		
Latitude mean*	4	9	10	9	5	3	7	11	6	0.26	0.16
Latitude SE*	0.1	0.8	0.2	0.3	0.2	0.2	0.1	0.4	0.2		
Inland tiles (%)	63	57	25	25	23	64	67	24	26	0.03	0.64
Elevation mean (m)	127	819	782	532	637	422	559	434	801	0.03	0.66
Elevation SE (m)	227	142	171	159	94	89	89	72	204		
Number of tiles	16	7	20	4	13	14	15	21	19		
Mean monthly burned area (%)	0.4	1.5	1.3	0.1	0.6	0.3	2.5	1.7	1.0		
SE monthly burned area (%)	0.1	1.0	0.5	0.2	0.1	0.2	0.8	0.4	0.3		

*Longitude and latitude units as in Fig. 3.
R^2 and *P*-value between these variables and mean monthly burned area percentage.
SE, standard error.

pixels increased significantly (9 pixel yr^{-1}). CL 5 mainly covered areas of open shrubland in southwest Asia, North Africa and Central America.

CL 6 presented a burned area peak in May. There was one significant downward trend in the number of burned pixels in January (statistic Z different from 0 with $P > 0.90$) and three significant upward trends in March, July and October. The slopes were quite small, except for July (52 pixel yr^{-1}). No annual trend was observed. CL 6 included mostly cropland and grassland, with tiles located in northern North America and northern Eurasia.

CL 7 had the largest burned area with a fire season from November to May and an interannual fire cycle. Trends were not observed for any month or annually. CL 7 was a mix of evergreen broadleaf forest, wood grassland and woodland. Tiles were situated in the equatorial region of Africa and South America.

CL 8 had a similar fire regime to CL 7 but with lower total burned area and no clear beginning or end of the fire season and no apparent interannual cycle. No significant temporal trends were observed. CL 8 covered mainly open and closed shrubland and savanna. Tiles were located in Australia, South Africa and southern South America.

CL 9 had a burned area peak in March–April. No trends were observed for any month but there was a significant annual decrease (−5 pixel yr^{-1}). This CL was broad mix of different land cover types with tiles located in Central America and southeast Asia.

Discussion

PC analysis provided identification of the main temporal burned area patterns: PC 1 and 2 accounted for annual cycles and PC 3 and 4 accounted for the semiannual patterns. Other PCs accounted for other periodicities, which were in general, less important in our CL.

The three main global fire seasons encountered were: CL 1–4 from June to December; CL 5, 6 and 9 from February to June; and CL 7 and 8 from October to March. Annual and semiannual patterns were more important than interannual in all CL, except for CL 4 and CL 5. Carmona-Moreno *et al*. (2005) presented a global three month fire season, but our results do not support the significance of a fire season for these areas. CL 4 corresponded to tiles with an extraordinary high burned area in 1997, apparently due to a strong El Niño event (Gutman *et al*., 2000; Wooster & Strub,

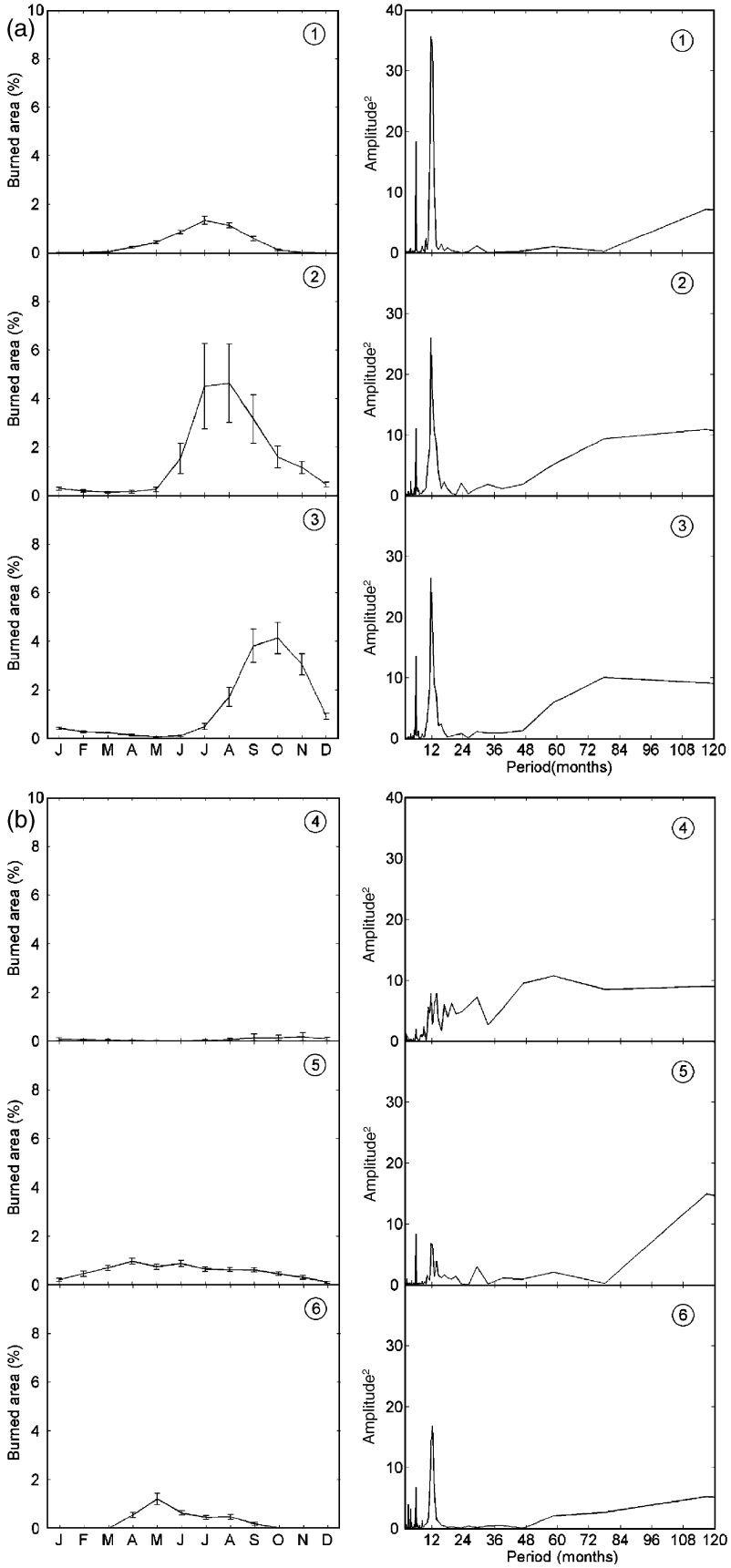

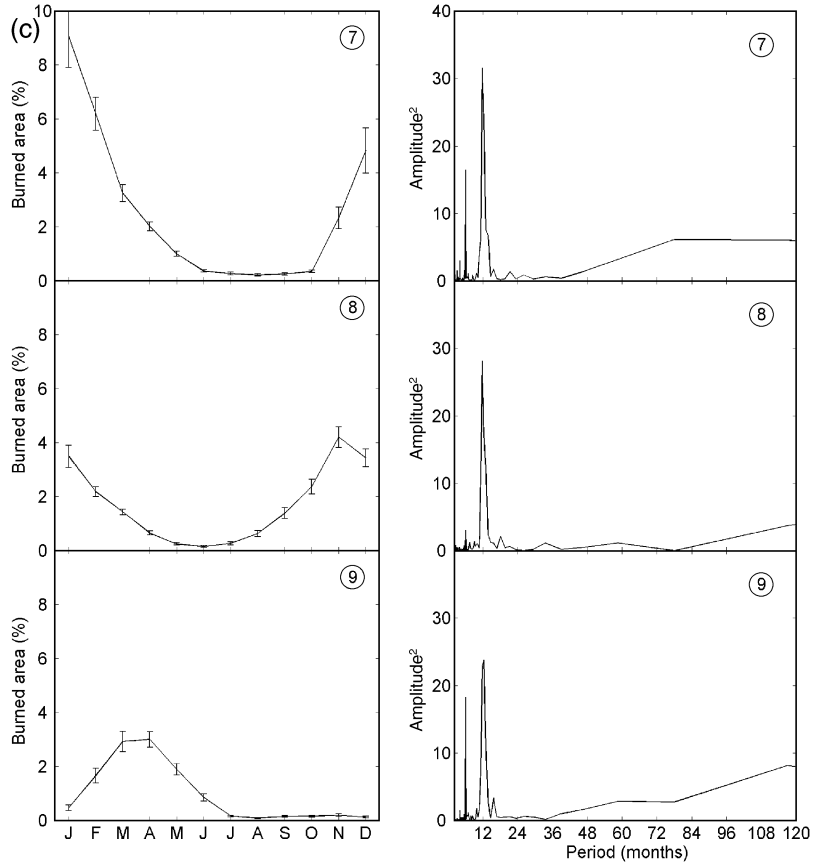

Fig. 4 Mean and standard error of percent monthly burned area (left) and periodogram or frequency of occurrence in months (right; $n = 234$) considering all tiles in each cluster 1–3 (a), 4–6 (b) and 7–9 (c).

2002). CL 5 showed unclear seasonality. Tiles, mainly open shrublands, were located in a semidesert environment with no apparent rainy season. CL 8 was the only one, out of all CL, that had an annual cycle, but did not have semiannual periodicity. Therefore, there was no clear fire season but instead CL 5 had a pattern where burned area increased and decreased gradually throughout the year. Interannual periodicities of 4–7 years were encountered for CL 2–4 and 7 but they are hard to corroborate since the 20-year time series has only three to five complete cycles.

The seasonal patterns presented in Fig. 4 nominally confirm those presented by Dwyer *et al*. (2000b). CL 7 coincide with the fire frequency of northern Africa provided by these authors and also Simon *et al*. (2004), which show a fire season from November to May. CL 2 shows similar results for southern Africa where fires occur in July–August, also matching Simon *et al*. (2004). CL 9 had patterns similar to Southern Asia and Central America in terms of fire season, although in our case higher fire frequencies were found for Southern Asia than for Central America and a more gradual change in the number of fires. CL 8 also showed similar results for Australia. Our results differed from Simon *et al*. (2004) for fire seasons from June to September. These differences can be explained because CL 8 included tiles from other continents than Simon *et al*. (2004) and because their data were based only on the year 2000. CL 1 and 6 showed similar results for Eurasia and North America. In their case, North America had a lower fire frequency than Eurasia, whereas in our case these areas were differentiated by latitude but not by continent. CL 3 agreed with their results for South America in showing a fire peak around September–October.

There was no significant global annual upward or downward trend in burned area but there were significant trends for specific areas of the world. CL 1 and 5 showed an upward burned area trend annually and for particular months. CL 9 showed an annual downward trend. CL 1 included areas in Eurasia and western North America which had the highest annual upward trend in the 20-year record with 24.2 pixel yr^{-1}. This trend was mainly due to the increase in burned area in June and July. Mouillot & Field (2005) also showed an increase in North America and Central Asia but a decrease for Europe. They provided burned area for

each decade grouping their data at continental scale by vegetation types. Therefore, it is difficult to compare their results with ours as our data were grouped in terms of fire frequency. CL 1 included southern Europe and northern Africa instead of Europe. For example, tile 2004 (Spain and northern Africa) increased fire frequency about 19% in the last decade. This increase was also found for Spain by Pausas (2004).

There was also no significant upward or downward global trend in the burned area for any individual month. The main trends at the CL level were upward for CL 1 (June and July) and 6 (July). In CL 1 the main fire season occurred in July and August (Fig. 4a), so the upward trend in June indicates an earlier start to the fire season. This pattern matches the results of Stocks *et al*. (1998) who studied how a warmer climate in the boreal forest could cause an increase in the fire danger in the summer and an earlier start of the fire season.

The global distribution of CL showed how tiles were principally grouped by land cover and more specifically by the proportional amount of savanna cover (Fig. 3 and Table 2). Although this vegetation type is secondary in all CL, burned area is higher where the extent of savanna in the CL is greater. This finding is supported by the fact that this biome has the highest fire risk (Mouillot & Field, 2005).

The relationship between latitude and burned area was not always clear. For example, CL 1 and 6 were at latitude 4 and had similar fire patterns but CL 2, 3 and 8 at latitude 10 corresponded to significantly different fire patterns (Fig. 4). Carmona-Moreno *et al*. (2005) used fire records grouped by latitude which can yield mixed groups of widely different fire frequencies. Also, mean and SE longitude shown in Table 2 must be regarded with caution as it is a circular variable, that is 0° and 360° longitude are equal. The CL spatial distributions we found differ from Dwyer *et al*. (2000a), who only considered the total number of fires for the year April 1992–March 1993, instead of monthly as in our data. Our input variables, derived from a longer temporal dataset, also account for seasonal differences when building the CL.

Higher elevations (Diaz-Delgado *et al*., 2004) and coastal areas have lower fire risk (Verdon *et al*., 2004) but based on our study the burned area is not different in these areas (Table 2). The expected differences were not observed probably because of compensating factors at our level of spatial analysis.

Conclusions and implications

Three major global fire seasons were found (1) from June to December for tropical and equatorial South America, equatorial and tropical South Africa, Madagascar, New Guinea and Indonesia, western North America and Eurasia (CL 1–4); (2) from February to June for Central America, North Africa, South Asia, northern North America and northern Eurasia (CL 5, 6 and 9) and (3) from October to March for the northern equatorial region of South America and Africa, southern South America, South Africa and Australia (CL 7 and 8). The temporal pattern in burned area followed mainly an annual cycle and secondly an important 6-month cycle. Interannual variations were more important than seasonal patterns in New Guinea, Indonesia and northern South America, southwest Asia, North Africa and Central America (CL 4 and 5).

Fires impact the global carbon cycle. They are a source of carbon to the atmosphere, if they are not compensated by biomass accumulation (Mouillot & Field, 2005). The burned area was not found to increase significantly in the last 20 years at the global scale but it did increase for the northern hemisphere in the mid-latitudes and subtropical areas of North America, Africa and southwest Asia. The burned area decreased in tropical southeast Asia and Central America. There was a summer increase in burned area in the mid-latitudes of the northern hemisphere and boreal areas. An earlier start of the fire season was also found for the mid-latitudes of the northern hemisphere.

Global fire patterns found in the 20 years of burned area records were distributed by land cover and the proportion of savanna land cover within the tiles. Latitude was not determinative as divergent fire patterns were encountered for various land cover areas at the same latitude.

Acknowledgements

A Fulbright Grant and the financial sponsorship of the Spanish Ministry of Education supported Daniel Isidoro. Ministry of Science and Technology 'Ramón y Cajal' Program supported David Riaño. The authors thank Goddard Space Flight Center and AVHRR Land Science team for producing and providing the NOAA-AVHRR Daily Tile PAL dataset. We thank George Scheer and Larry Ross of the CSTARS Lab at UC Davis for computer support. Linguistic assistance from Julia Marcia Medina is also acknowledged.

References

Anderson HE (1982) *Aids to determining fuel models for estimating fire behavior*. General Technical Report INT-122, USDA, Forest Service, Ogden, UT.

Barbosa PM, Grégoire JM, Pereira JMC (1999) An algorithm for extracting burned areas from time series of AVHRR GAC data applied at a continental scale. *Remote Sensing of Environment*, **69**, 253–263.

Box GEP, Jenkins GM, Reinsel GC (1994) *Time Series Analysis: Forecasting and Control*. Prentice Hall, Upper Saddle River, NJ.

Carmona-Moreno C, Belward A, Malingreau JP *et al*. (2005) Characterizing inter-annual variations in global fire calendar using data from earth observing satellites. *Global Change Biology*, **11**, 1537–1555.

Chuvieco E, Salas FJ, Carvacho L *et al*. (1999) Integrated fire risk mapping. In: *Remote Sensing of Large Wildfires in the European Mediterranean Basin* (ed. Chuvieco E), pp. 61–84. Springer-Verlag, Berlin.

De Fries RS, Hansen M, Townshend JRG *et al*. (1998) Global land cover classifications at 8 km spatial resolution: the use of training data derived from Landsat imagery in decision tree classifiers. *International Journal of Remote Sensing*, **19**, 3141–3168.

Diaz-Delgado R, Lloret F, Pons X (2004) Spatial patterns of fire occurrence in Catalonia, NE, Spain. *Landscape Ecology*, **19**, 731–745.

Dwyer E, Gregoire JM, Malingreau JP (1998) A global analysis of vegetation fires using satellite images: spatial and temporal dynamics. *Ambio*, **27**, 175–181.

Dwyer E, Pereira JMC, Gregoire JM *et al*. (2000a) Characterization of the spatio-temporal patterns of global fire activity using satellite imagery for the period April 1992 to March 1993. *Journal of Biogeography*, **27**, 57–69.

Dwyer E, Pinnock S, Gregoire JM *et al*. (2000b) Global spatial and temporal distribution of vegetation fire as determined from satellite observations. *International Journal of Remote Sensing*, **21**, 1289–1302.

Gilbert RO (1987) *Statistical Methods for Environmental Pollution Monitoring*. Van Nostrand Reinhold Co., New York.

Gregoire JM, Tansey K, Silva JMN (2003) The GBA2000 initiative: developing a global burnt area database from SPOT-VEGETATION imagery. *International Journal of Remote Sensing*, **24**, 1369–1376.

Gutman G, Csiszar I, Romanov P (2000) Using NOAA/AVHRR products to monitor El Nino impacts: focus on Indonesia in 1997–98. *Bulletin of the American Meteorological Society*, **81**, 1189–1205.

Hao WM, Liu MH (1994) Spatial and temporal distribution of tropical biomass burning. *Global Biochemical Cycles*, **8**, 495–503.

IPCC (2000) *Special report emissions scenarios, WMO & UNEP*. http://www.grida.no/climate/ipcc/spmpdf/sres-e.pdf.

Justice CO, Giglio L, Korontzi S *et al*. (2002) The MODIS fire products. *Remote Sensing of Environment*, **83**, 244–262.

Kasischke ES, Penner JE (2004) Improving global estimates of atmospheric emissions from biomass burning. *Journal of Geophysical Research-Atmospheres*, **109**, 1–9.

Lanly JP (1982) *Tropical Forest Resources*. FAO, Rome.

Levine JS (1996) *Biomass Burning and Global Change*. The MIT Press, Cambridge, MA.

Moreno Ruiz JA, Barbosa PM, Carmona-Moreno C *et al*. (1999) *Glints-BS Global Burn Scar Detection System: Functional Description and User Manual Document, JRC-SAI*. Global Vegetation Monitoring Unit, Ispra, Italy.

Mouillot F, Field CB (2005) Fire history and the global carbon budget: a 1 degrees $\times$ 1 degrees fire history reconstruction for the 20th century. *Global Change Biology*, **11**, 398–420.

NGDC (1993) *5 Minute Gridded World Elevation*. NGDC Data, Boulder, CO.

Pausas JG (2004) Changes in fire and climate in the eastern Iberian Peninsula (Mediterranean basin). *Climatic Change*, **63**, 337–350.

Peiris DR, McNicol JW (1996) Modelling daily weather with multivariate time series. *Agricultural and Forest Meteorology*, **79**, 219–231.

Piwowar JM, Ledrew EF (2002) ARMA time series modelling of remote sensing imagery: a new approach for climate change studies. *International Journal of Remote Sensing*, **23**, 5225–5248.

Rouse JW, Haas RW, Schell JA *et al*. (1974) *Monitoring the Vernal Advancement and Retrogadation (Greenwave Effect) of Natural Vegetation*. NASA/GSFCT, Greenbelt, MD, USA.

Roy DP, Jin Y, Lewis PE *et al*. (2005) Prototyping a global algorithm for systematic fire-affected area mapping using MODIS time series data. *Remote Sensing of Environment*, **97**, 137–162.

Ryan KC (2002) Dynamic interactions between forest structure and fire behavior in boreal ecosystems. *Silva Fennica*, **36**, 13–39.

Seiler W, Crutzen PJ (1980) Estimates of gross and net fluxes of carbon between the biosphere and the atmosphere from biomass burning. *Climatic Change*, **2**, 207–247.

Simon M, Plummer S, Fierens F *et al*. (2004) Burnt area detection at global scale using ATSR-2: the GLOBSCAR products and their qualification. *Journal of Geophysical Research-Atmospheres*, **109**, 1–16.

Stocks BJ, Fosberg MA, Lynham TJ *et al*. (1998) Climate change and forest fire potential in Russian and Canadian boreal forests. *Climatic Change*, **38**, 1–13.

Stroppiana D, Pinnock S, Gregoire JM (2000) The global fire product: daily fire occurrence from April 1992 to December 1993 derived from NOAA AVHRR data. *International Journal of Remote Sensing*, **21**, 1279–1288.

Tansey K, Gregoire JM, Stroppiana D *et al*. (2004) Vegetation burning in the year 2000: global burned area estimates from SPOT VEGETATION data. *Journal of Geophysical Research-Atmospheres*, **109**, 1–22.

Townshend J, Justice C, Li W *et al*. (1991) Global land cover classification by remote sensing: present capabilities and future possibilities. *Remote Sensing of Environment*, **35**, 243–255.

Trewartha GT, Robinson AH, Hammond EH (1961) *Fundamentals of Physical Geography*. Mc Graw-Hill Book Inc., New York.

Verdon DC, Kiem AS, Franks SW (2004) Multi-decadal variability of forest fire risk – eastern Australia. *International Journal of Wildland Fire*, **13**, 165–171.

Wooster MJ, Strub N (2002) Study of the 1997 borneo fires: quantitative analysis using global area coverage (GAC) satellite data. *Global Biogeochemical Cycles*, **16**, 1–12.

